*Article*

# The Impact of High-Density Airborne Observations and Atmospheric Motion Vector Observation Assimilation on the Prediction of Rapid Intensification of Hurricane Matthew (2016)

**Xinyan Lyu [1,2] and Xuguang Wang [2,*]**

[1]  National Meteorological Center, China Meteorological Administration, Beijing 100081, China; lvxy@cma.gov.cn
[2]  School of Meteorology, University of Oklahoma, Norman, OK 73072, USA
[*]  Correspondence: xuguang.wang@ou.edu

**Abstract:** Tropical cyclone rapid intensification (RI) prediction still remains a big international challenge in numerical weather prediction. Hurricane Matthew (2016) underwent extreme and non-classic RI, intensifying from a Category 1 storm to a Category 5 hurricane within 24 h under a strong vertical shear environment. However, most models failed to capture this RI, and limited or no inner core, and outflow observations were assimilated in the NWS operational HWRF Model before the onset of RI for Matthew (2016). The goals of the study are to (1) explore the best way to assimilate the High-Density Observations (HDOB, including FL and SFMR) and AMV data; (2) study the impact of assimilating these observations on the analysis of both the inner-core and outflow structures; and (3) examine the impact of assimilating these data on the prediction of RI for Matthew. The main results are as follows: (1) With proper pre-processing of the HDOB observations and by using a 4DEnVar method, the inner-core structure analysis was improved. And the RI prediction is more consistent with the best track without spin-down for the first 24 h. Assimilating CIMMS AMV observations on top of the HDOB observations further improves both the track and intensity forecasts. Specifically, both the magnitude and timing of the peak intensity are further improved. (2) Diagnostics are conducted to understand how the assimilation of these different types of observations impacts RI prediction. Without assimilating HODB and AMV data, baseline experimentover-predict the intensification rate during the first 18 h, but under-predict RI after 18 h. However, the assimilation of FL and SFMR and CIMMS AMV correctly weakens the upper-level outflow and improves the shear-relative structure of the inner-core vortex, such as reducing the low-level moisture in the downshear left quadrant. The deep convection on the downshear side is weaker than baseline for the first 18 h but keeps enhancing, later moving cyclonically to the USL quadrant, and then causes more subsidence warming, maximizing in the USL quadrant and the maximum wind increases faster. Moreover, the rapid intensification rate is much more consistent with the best track and the forecast skill of RI is improved. Therefore, 4DEnVar assimilation with proper pre-processing of the high-density observations can indeed correct the shear-relative moisture and structural distributions of both the inner core and environment for TCs imbedded in the stronger shear, which is important for shear-TC RI prediction.

**Keywords:** assimilation; tropical cyclone; hurricane; strong vertical shear; rapid intensification

## 1. Introduction

Numerical weather prediction models have been constantly improving in terms of tropical cyclone (TC) track predictions over the last decades. However, the progress of TC intensity prediction cannot keep pace with track prediction. Especially TC rapid intensification (RI), typically defined as a maximum wind increase of 30 kt over 24 h [1], still remains a big challenge in numerical weather prediction models [2,3], and large TC intensity forecast errors usually occur during episodes of RI [4]. NHC (National Hurricane

Center) takes improving of the RI prediction as one of its top priorities for the tropical meteorology research community [5]. In particular, the annual number of RI events in global offshore areas has experienced a significant increase from 1980 to 2020 [6]. The RI perdition skill however is still limited for models.

The environmental vertical wind shear (VWS) is one of the most critical factors affecting tropical cyclone intensification and it is widely accepted that strong VWS usually inhibits TC intensification [7–11]. The "ventilation effect" is one of the direct reasons that VWS limits TC intensification by breaking the warm core or venting moisture and energy out of the TC core and transporting low-entropy air into the TC core [12–16]. However, there is still a large number of TCs that intensify rapidly under moderate or strong vertical wind shear [17–20]. VWS can also influence TC intensity predictability [21,22]. The uncertainty of TC intensity forecast arises with an increase of vertical wind shear [22,23], and the intensity forecast error of TCs under moderate vertical wind shear is usually significant [24]. In another word, the prediction of RI under moderate or strong shear is much more difficult.

The shear-relative quadrant distributions of the impacting factors (e.g., inflow, moisture) are crucial for TC intensity changes under stronger or moderate shear. Gu et al. studied the evolution of the low-level tangential wind near the eyewall of an idealized simulated mature TC in a unidirectional shear flow, and showed that the boundary layer inflow on downshear side is crucial for the evolution of the left-of-shear tangential wind and TC intensity. A TC still intensifies under stronger VWS as long as the boundary inflow on the downshear side (especially in the DSL quadrant) is stronger [25,26]. Hazelton et al. studied the early intensification of Hurricane Dorian using the high-resolution ensemble of the hurricane analysis and forecast system (HAFS) and demonstrated that the low-level moisture and upper-level divergence are much higher in the northeastern part of the TC for intensification members [27]. Zawislak et al. and Leighton et al. (2018) showed that the increase of moisture on the downshear side in the lower troposphere was favorable for the rapid intensification of hurricane Edourd (2014) [28,29]. Satellite-based observations showed that the shear-relative distribution of moisture determines its impact on TC intensity change [30–32]. Rios-Berrios et al. investigated the intensification of hurricanes Katia (2011) and Ophelia (2011) under moderate VWS using the ensemble approach and found that the shear-relative distribution of moisture in the lower and mid-troposphere can have a significant impact on hurricane intensification. They suggested that moisture observations may help reduce the uncertainty in the forecast of weak and sheared TCs [18,19]. Additionally, some studies further show that asymmetric convection burst (CB) can trigger RI of a TC in moderate VWS, especially under a favorable shear-relative distribution of impacting factors. The CB on the downshear side is favorable for RI of TCs embedded in moderate VWS, especially CB in the DSL quadrant [33,34]. Observational studies' results showed that 92% of downshear inner-core lightning bursts occurred in TCs that remained steady or intensified under a moderate shear environment [35]. Molinari and Vollaro showed that a convective cell enhanced in the DSL quadrant and moved cyclonically and inward to the RMW during the period of rapid intensification of Gabrielle (2011) under stronger VWS (12–13 m/s) [36]. But some studies find that the CB on left side can trigger RI much easier than on right side [18,37]. Wadler et al. further found significant differences in convection on the upshear side between intensification and steady TCs under a moderate shear by using NOAA P-3 tail Doppler radar, especially the convection in the USL quadrant is much stronger in intensified cases than steady cases [38]. Chen and Gopalakerishnan show that subsidence warming is maximum on the upshear side when CBs are concentrated in the DSL and USL quadrants and then is advected toward the low-level TC center, leading to RI [17]. Zhang and Tao showed that the vortex tilt is determined by the location of deep convection, and the vortex tilt begins to reduce and TC intensification occurs after the tilt angle reaches 90° to the left of the environmental shear [22]. Fischer et al. showed that anomalously cold infrared and 85 GHz brightness temperatures in the upshear quadrants of the TC are associated with increased rates of TC intensification [39]. Leighton et al. showed that the shear-relative distribution of the upper-level flow and low-level moisture

is important for the distribution of a TC's deep convection, and vortex tilt and asymmetry reduce rapidly as the deep convection wraps around from the downshear side to the USL quadrant, and that under these conditions hurricane Edouard (2014) began RI [28]. Chen et al. explored the simultaneous effect of vertical wind shear (VWS) and low-level mean flow (LMF) on tropical cyclone (TC) structure evolution and showed that a LMF directed toward the left-of-shear orientation favors TC intensification by promoting convection in the upshear inner core. Then enhancement of the symmetric inner-core convection favors TC intensification [37,40]. Although the above results are somehow different, the shear-relative distributions of impact factors (the moisture and inflow) are very important for the convection burst (CB) that triggers TC intensification. In order to better understand the impact of the shear-relative distribution on tropical cyclone intensity change, this study will further discuss how the differences in shear-relative quadrant distributions between assimilation and baseline experiments impact inner-core convection and subsequent intensity change.

High-density airborne observations (HDOB), including Stepped Frequency Microwave Radiometer (SFMR) and flight-level (FL) observations are collected through the NOAA WP-3D aircraft [41]. The SFMR observations are sampled at the surface, and the FL observations are usually centered between 2000 km and 3000 km in altitude (700–800 hPa). The SFMR wind observations are widely used to validate or estimate the maximum surface wind speed for hurricanes [39,42]. Assimilating SFMR observations improves both the surface inner-core TC structures (including the radial wind pattern in the mid- to low levels) and the intensity forecast [43–45]. FL observations have been used in TC center estimation and TC inner-core structure assimilation and validation [46–48]. Assimilating FL observations can produce corrections to the wind field (including radial inflow and outflow of TC) and also provide more realistic low-level inner-core TC structures, which can help improve intensity predictability [45].

The Atmospheric Motion Vector (AMV) observations are wind observations derived by tracking clouds or areas of water vapor in consecutive geostationary satellite images (mainly from the VIS, IR window, and WV absorption band). In recent years, as the algorithms of AMV and satellite observation have been much improved, higher quality and higher resolution (spatially and temporally) AMV data can be provided. Especially the "enhanced" AMV observations used in this study have been produced by the Cooperative Institute for Meteorological Satellite Studies (CIMSS) [31,32,49]. The CIMSS AMVs are designed to have higher density, larger coverage, and better quality as compared to the operationally produced AMVs provided by the National Environmental Satellite, Data, and Information Service (NESDIS) [49]. AMVs are widely used to analyze the mid–upper level environment of TCs [50,51], especially the outflow structure and strength. Early studies found that assimilating the CIMSS AMVs can have positive impacts on the TC track and intensity predictions [31,32,52], by improving the analysis of the upper-level environment (including the outflow structure of TC) [53,54], and providing some information about the near inner-core environment [45,49]. Therefore, assimilating HDOB and AMVs may correct the shear-relative distributions of the impact factors (e.g., low-level inflow of the upper-level outflow structures) and further improve RI prediction under strong shear.

Although both HDOB and AMV observations have high-density and can provide useful information for hurricane intensity forecasting, the optimal way to assimilate these data is not clear. The first goal of the study is to explore the three-dimensional ensemble-variational data assimilation method (3DEnVar) [55–58] and four-dimensional ensemble-variational data assimilation method (4DEnVar,) [59,60] for the assimilation of the high density airborne and AMV observations. Earlier studies demonstrate that 4DEnVar generally has better performance than 3DEnVar due to the ability of 4DEnVar to estimate flow-dependent background error covariances [61,62]. The high data density may violate the assumption of independent measurement errors. The work of Liu and Rabier showed that the analysis quality decreases if the density of the observational data set is too large and spatial error correlations are neglected [58]. Therefore, pre-processing is performed for the high-density observations, which can reduce computational costs and also improve

assimilation performance. Data thinning and superobbing are two pre-processing methods usually used for high-density observation. Data thinning can reduce the spatial or spectral resolution by selecting a reduced set of locations or channels, while data superobbing reduces the spatial or spectral resolution by combining or averaging over locations or channels. The second goal of the study therefore is to explore the optimal pre-processing method for high-density HDOB and AMV. The third goal of the study is to examine the hypothesis that the limited skill of numerical prediction of RI is partly because the analysis cannot describe the asymmetric distribution of the aforementioned impact factors. Hurricane Matthew (2016) is a typical case that intensified extremely rapidly under a moderate shear. Given the observations of the HDOB and AMV are available during the onset period of RI, and they directly or indirectly sample the shear-relative environmental factors (inflow, moisture, outflow) near the inner core, this study will focus on addressing the aforementioned hypothesis through examining the impacts of assimilating the HDOB (near the TC core in low-level) and AMV (mainly outside of the TC in upper-level) data on Hurricane Matthew's RI prediction.

## 2. Overview of Hurricane Matthew

Hurricane Matthew was the strongest storm of the 2016 Atlantic Hurricane Season. Matthew became a tropical storm at 1200 UTC 28 September over the sea on the west–northwest side of Barbados. It gradually strengthened within an environment of west–southwesterly $850-200$ mb vertical wind shear of about 20 kt while moving westward and attained a hurricane status by 1800 UTC 29 September (Figure 1a). For the next 24 h, Matthew rapidly intensified from a Category 1 to a Category 5 hurricane within 24 h under a moderate vertical wind shear of about 20 kt (Figure 1b), which is usually believed to be unfavorable for intensification. It reached its peak intensity of 145 kt (1 kt $\approx$ 0.5144 m s$^{-1}$ at 0000 UTC on 1 October. Its intensity increased by 75 kt over 24 h. Therefore, Matthew underwent an unexpected 24 h period of extreme rapid intensification (RI: an increase of maximum sustained surface winds at least 30 kt (about 15 m s$^{-1}$; in a 24 h period), Kaplan et al., 2010) under moderate vertical wind shear with little change in direction between 0000 UTC on 30 September and 0000 UTC on 1 October. Matthew became the southernmost Category 5 hurricane in the Atlantic basin. After rapid intensification, Matthew began to weaken slowly, but it still maintained Category 5 status for a long time (4 days). However, most operational models failed to capture this RI, including both the consensus model and the individual members. No model could predict Matthew's RI period either before or during the episode [63], and NHC official intensity forecasts had errors much greater than the mean official errors for the previous 5-year period at all forecast times and contained a pronounced low bias. Therefore, more work should be performed to improve the RI predictability under a moderate vertical wind shear.
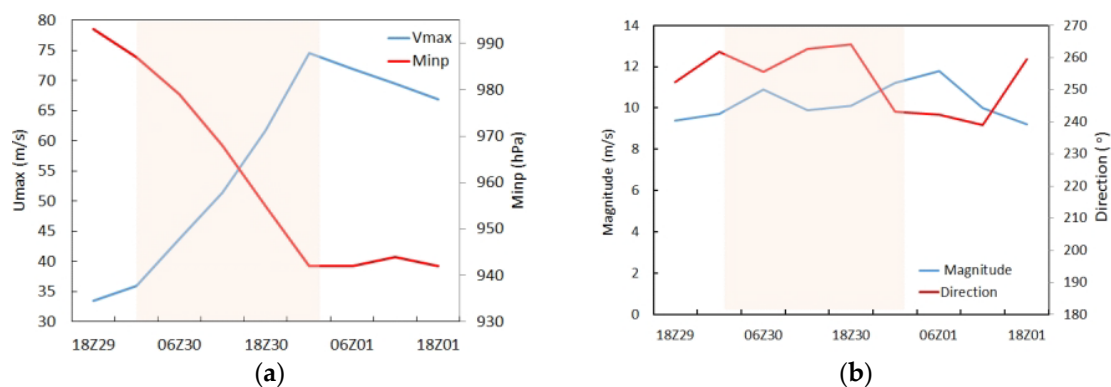


**Figure 1.** (**a**) The best track maximum sustained surface wind (blue, unit: m/s) and minimum central pressure curve (red, unit: hPa) for Hurricane Matthew; (**b**) the magnitude (blue line) and direction (red line) of the environmental vertical wind shear between 200 and 850 mb (the data are from SHIPs).

### 3. Model, Observational Data, and Experimental Design

*3.1. HWRF Model Configurations and the Assimilation System*

The HWRF Model was developed by the Environmental Modeling Center (EMC) in collaboration with the Geophysical Fluid Dynamics Laboratory (GFDL) and the University of Rhode Island (URI) based on the Weather Research and Forecasting (WRF) Model infrastructure and the NonHydrostatic Mesoscale Model (NMM) dynamic core. A horizontal grid spacing of 0.135°/0.045°/0.015° (approximately 18/6/2 km) for the outermost/intermediate/innermost domains is used for the well-developed hybrid DA system in this study, which is similar to that used in the operational HWRF. The outermost, intermediate, and innermost domains are configured with 288 × 576, 304 × 604, and 265 × 472 horizontal grid points, respectively. There are 61 vertical levels, and the model top is at 2 hPa following the operational HWRF. The physics parameterization schemes used in this study follow those used in the 2016 operational HWRF (details can be found in Table 1 of Lu's study [43]).

**Table 1.** Experimental design for Hurricane Matthew (2016).

| Exp. Name | General Information | DA Method | Pre-Pro | Additional Obs Assimilated |
|---|---|---|---|---|
| Baseline | Background: 6-h control forecast initialized from the GSI-based, continuously cycled, dual-resolution hybrid ensemble-variational (EnVar) DA system for HWRF valid at 1800 UTC 29 September 2016. Physics: H216 Physics + Modified turbulent mixing parameterization Observations: Operational HWRF observations (conventional obs., satellite radiances, et al.) | 4DEnVar | No | No |
| 3DEV | | 3DEnVar | No | |
| 4DEV | | 4DEnVar | No | |
| 4DEV-thin | | 4DEnVar | Thinning | |
| 4DEV-sob | | 4DEnVar | Sob | FL and SFMR CIMSS AMV |

The GSI-based, continuously cycled, dual-resolution hybrid ensemble–variational (EnVar) DA system for HWRF, developed by Lu et al. [44], is used in this study. At the initial cycle of a tropical storm, a 40-member 18/6 km doubly nested HWRF ensemble and a single deterministic 18/6/2 km triply nested HWRF control are initialized from the Global Forecast System (GFS) ensemble and control analyses, respectively. All analyses are from the National Centers for Environmental Prediction (NCEP) operational GFS hybrid DA system [58,59]. Then, vortex relocation is performed on both the ensemble and control forecasts, and vortex modification is only performed on the control forecast when inner-core observations are unavailable. More details about the DA system can be found in section 2 of Lu et al. [43].

*3.2. The Observational Data*

Limited or no inner-core and outflow observations were assimilated in the NWS operational HWRF Model before the onset of RI for Matthew (2016). Only the inner-core and near inner-core HDOB (Figure 2a), together with the enhanced CIMSS AMVs, were available before the onset of RI for Matthew (2016), aside from satellite radiance. These observations are assimilated to provide a realistic three-dimensional analysis of the storm and its environment.

Figure 2b shows the vertical distributions of the HDOB (including FL and SFMR) and AMV observations collected during this mission of Matthew. The greatest number of AMV observations generally concentrates in the upper-level between 400 and 150 hPa. The

greatest number of FL observations is mainly around 850 hPa, and some are at higher levels (around 700 hPa) within the inner core. Therefore, HDOB and CIMSS AMV together can provide three-dimensional sampling of the TCs, including the surface, inner cores, outflow layer, and environment.
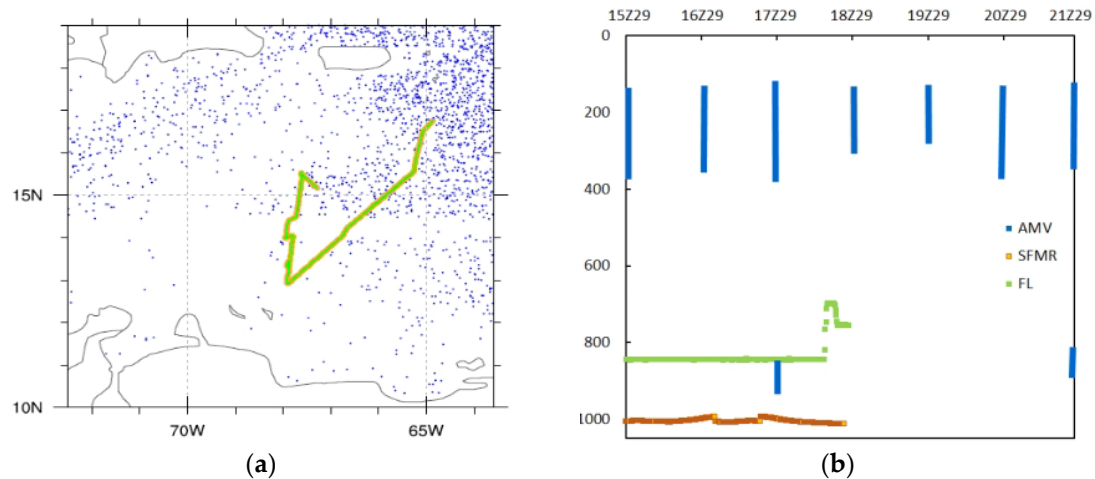


**Figure 2.** The distribution of HODB (FL: green; SFMR: brown) and AMV (blue) observations assimilated, valid at 1800 UTC 29 Sep 2016 during Hurricane Matthew. (**a**) Horizontal distribution; (**b**) vertical distribution.

### 3.3. Experimental Design

Experiments are initialized six hours before the onset of RI for Hurricane Matthew, valid at 18 UTC on 29 September 2016. The background is from our 2016 near real-time experiment with the advanced hybrid EnVar DA system (Lu et al., 2017a, b). The basic model physics and dynamic configurations follow the 2016 operational HWRF with ocean coupling turned on, except for a modified turbulent mixing parameterization scheme developed by Ping Zhu et al. (2016). As shown in the paper by Lu et al. (2019), this parameterization scheme is found to help build up the secondary circulation faster and can significantly improve the TC intensity forecast by eliminating the unrealistic discontinuity in the vertical diffusion profile.

To investigate the optimal pre-processing and DA method of HDOB (FL and SFMR) and AMV observations, as discussed earlier, five experiments are conducted in this reporting period (Table 1). Details for each experiment are described below. (1) The experiment Baseline does not assimilate HDOB and AMV whereas other experiments do. (2) Experiment 3DEV is the experiment that assimilates FL, SFMR, AMV, and other observations using 3DEnVar. (3) Experiment 4DEV is the same as 3DEV except that 4DEnVar DA is used instead of 3DEnVar. Together with 3DEV, this experiment 4DEV is designed to find the optimal DA method for the HDOB and AMV observation assimilation. (4) Experiments 4DEV-thin and (5) 4DEV-sob are the same as 4DEV experiments except that the observations are pre-processed through thinning (picking the center value of a certain prism) and superobbing (averaging over a certain prism), respectively. These experiments are conducted to investigate the optimal pre-processing methods for HDOB and AMV data.

## 4. Results of Experiments

### 4.1. Impact of DA Methods (3DEnVar vs. 4DEnVar)

Figure 3 depicts the evolution of the maximum wind speeds for the 3DEV and 4DEV experiments, as outlined in Table 1. Initially, the TC intensity is much stronger than the observations, and a spin-down issue occurs when both HDOB and AMV are assimilated using 3DEnVar. Further investigations reveal that this spin-down issue occurs specifically when HDOB (both FL and SFMR) data are assimilated. Additionally, the 3DEV analysis reveals a spurious secondary eyewall (Figure 4a), along with a spurious eyewall replacement pro-

cess occurring (Figure 4c). Eyewall replacement processes typically entail rapid structural changes in a tropical cyclone, often resulting in a decay. However, observations during this period do not support the occurrence of a real eyewall replacement (Stewart, 2017). Therefore, this short-term spin-down in 3DEV is attributed to a spurious secondary eyewall created during HDOB assimilation. Furthermore, the intensity has increased to 42 h forecast period; the intensifying time is longer that the observations.
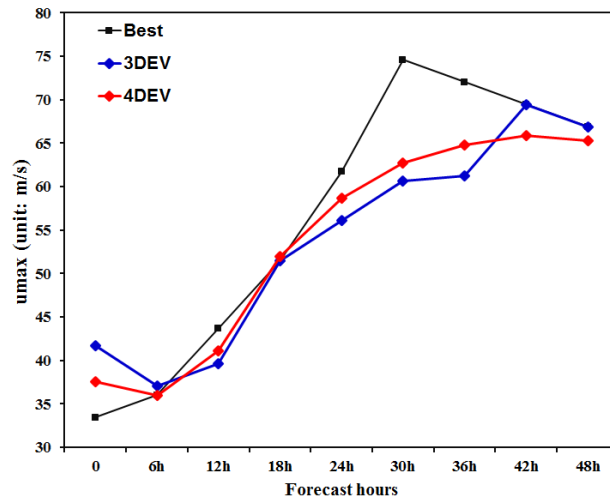


**Figure 3.** Hurricane Matthew's maximum wind forecasts for experiments 3DEV (blue line) and 4DEV (red line, described in Table 1) initialized from 18 UTC on 29 September 2016; the black line is for the intensity change of the best track.

However, in comparison to the results of 3DEV, the spuriously strong initial intensity is mitigated, and spin-down is alleviated by the flow-dependent 4DEnVar (Figure 3); 4DEnVar can create a more realistic analysis of the inner-core structure (Figure 4b), with the spurious secondary eyewall nearly disappearing. Consequently, the 4DEnVar DA method can alleviate the spin-down (Figure 4b,d), resulting in TC intensity forecasts that are more consistent with observations. This improvement in 4DEnVar over 3DEnVar for the temporally unevenly distributed observational DA is consistent with the findings of Lu et al. (2017a). However, the initial intensity remains slightly stronger than observed, and the spin-down still exists even with 4DEnVar. And the time of the peak intensity is later and the intensification time exceeds that of the observations.
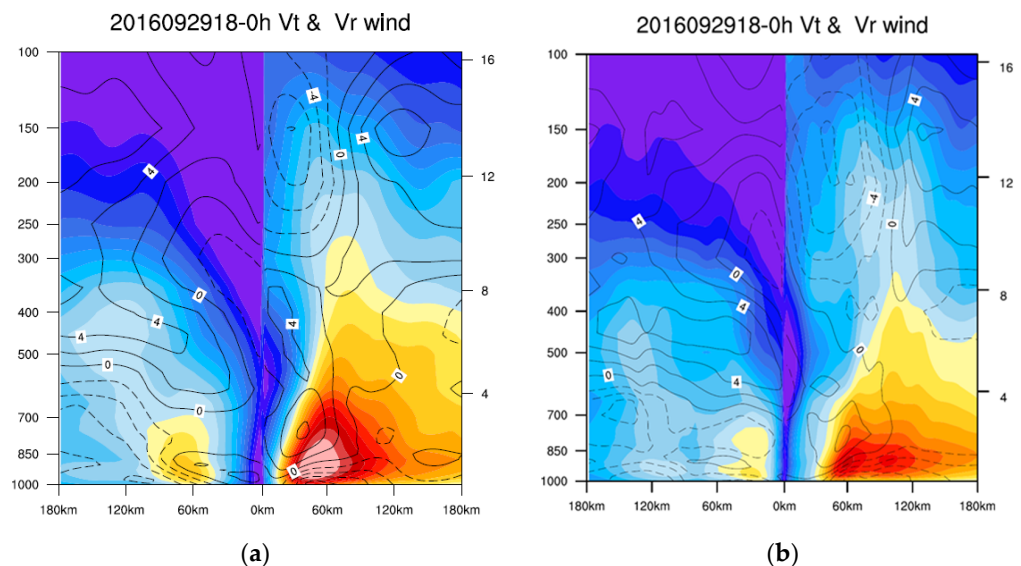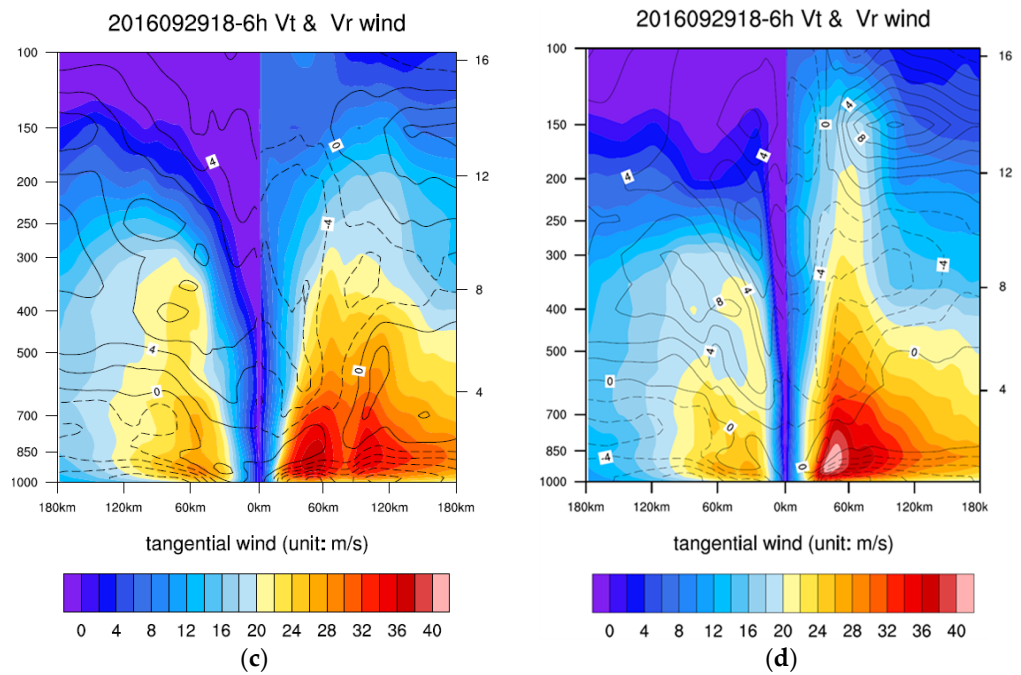


**(a)**             **(b)**

**Figure 4.** *Cont.*

**Figure 4.** The height–distance (with TC center) profile of radial wind (contour: unit: m/s) and tangential wind (shaded, unit: m/s) for the experiments of 3DEV (**a**,**c**) and 4DEV (**b**,**d**). (**a**,**b**) Are the analysis, (**c**,**d**) are the 6 h forecast.

## 4.2. Impacts of Pre-Processing (Thinning vs. Superobbing)

As mentioned in the previous section, the initial intensity remains slightly stronger than observed and a spin-down issue still exists in experiment 4DEV. Additionally, considering the high spatial (3 km) and temporal density (30 s interval) and uneven spatial distribution of HDOB observations used in this particular case (Figure 2), we hypothesize that a better pre-processing method, such as thinning or superobbing, may be helpful in improving the analysis structure and alleviating the forecast spin-down issue. Two of the experiments (4DEV-thin and 4DEV-sob) are conducted to verify our hypothesis (Figure 5).
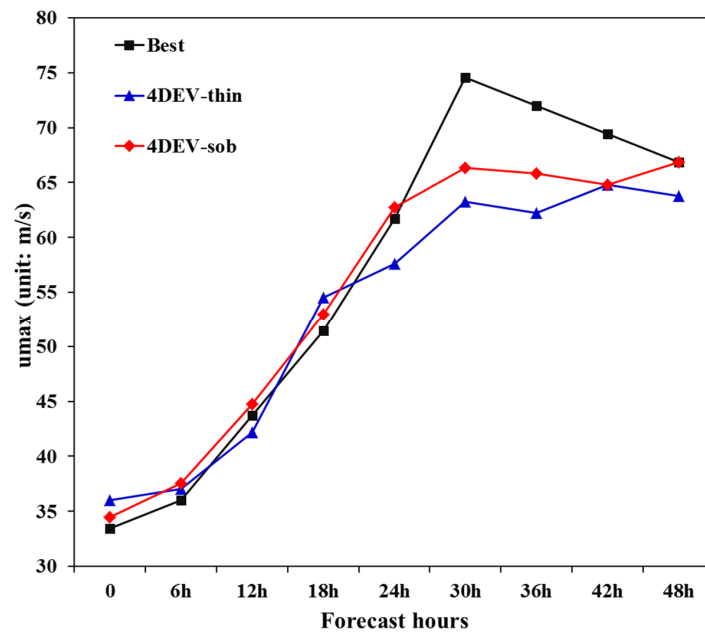


**Figure 5.** Vmax forecasts for experiments 4DEV-thin (blue line) and 4DEV-sob (red line, described in Table 1) initialized from 18 UTC 29 September 2016 during Hurricane Matthew; the black line is for the intensity change of the best track.

Further experiments based on the 4DEnVar DA show that both superobbing and thinning can help further reduce the spuriously strong initial Vmax analysis and produce a more realistic inner-core structure analysis without the appearance of a spurious secondary eyewall (Figure 6), thus alleviating the spin-down issue. These results suggest that proper pre-processing is necessary for the high-density HDOB observations. Moreover, the sensitivity experiments indicate that the initial TC intensity closely aligns with observation, and RI predictions are more consistent with observations for the first 24 h in experiment 4DEV-sob. However, while the initial TC intensity remains slightly stronger in 4DEV-thin, the peak intensity is more significantly under-predicted compared to observations than 4DEV-sob. Therefore, the superobbing outperforms thinning (both within over 12 km × 12 km × 20 hPa prisms). Overall, by using proper pre-processing, such as superobbing, of the HDOB observations with a 4DEnVar DA method, the inner-core structure analysis can be improved, the spurious secondary eyewall can be eliminated, and RI prediction can be made more consistent with the best track for the first 24 h, resulting in more accurate RI predictions, including both the magnitude and timing of the peak intensity.
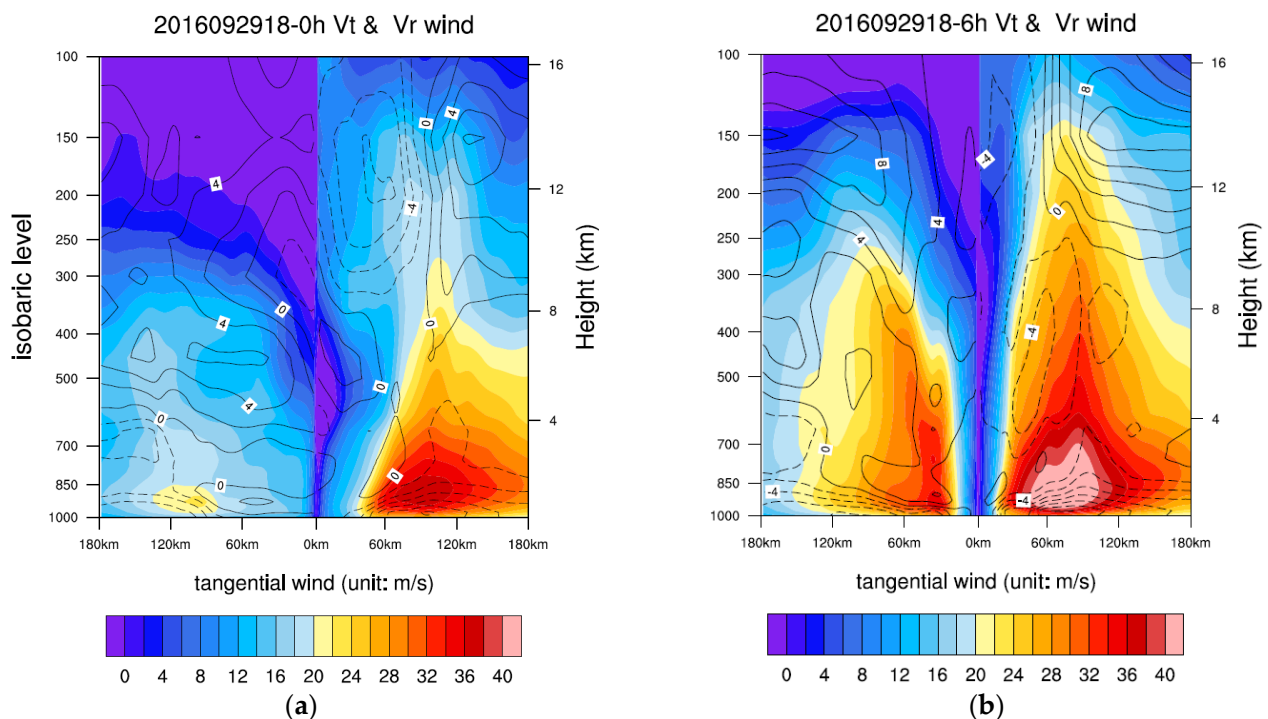


**Figure 6.** The height–distance (with TC center) profile of radial wind (contour: unit: m/s) and tangential wind (shaded, unit: m/s) for the experiment of 4DEV-sob. (**a**) Analysis; (**b**) 6 h forecast.

## 5. Impact of Assimilating HDOB and AMV on RI Prediction

### 5.1. The Impact of Assimilating HDOB and AMV on Inner-Core and Outflow Structures in Analysis Fields (Shear-Relative Distribution)

In this section, based on the comparisons between experiments Baseline and 4DEV-sob (detail sees Table 1), the impact of assimilating HDOB and AMV on the inner-core and outflow structures in the analysis fields is discussed.

Overall, assimilating HDOB and AMV weakens the upper-level outflow (Figure 7a) and low-level moisture inflow (Figure 7b) in the analysis fields. Moreover, further analysis reveals that the major differences in the analysis fields are in the USL and DSL quadrants (the region near the hurricane center is divided into four quadrants relative to the deep-layer shear (between 200 hPa and 850 hPa): DSL is the downshear left; DSR is the downshear right; USR is the upshear right; USL is the upshear left). Therefore, the following analysis will mainly focus on the data's impact on the USL and DSL quadrants.
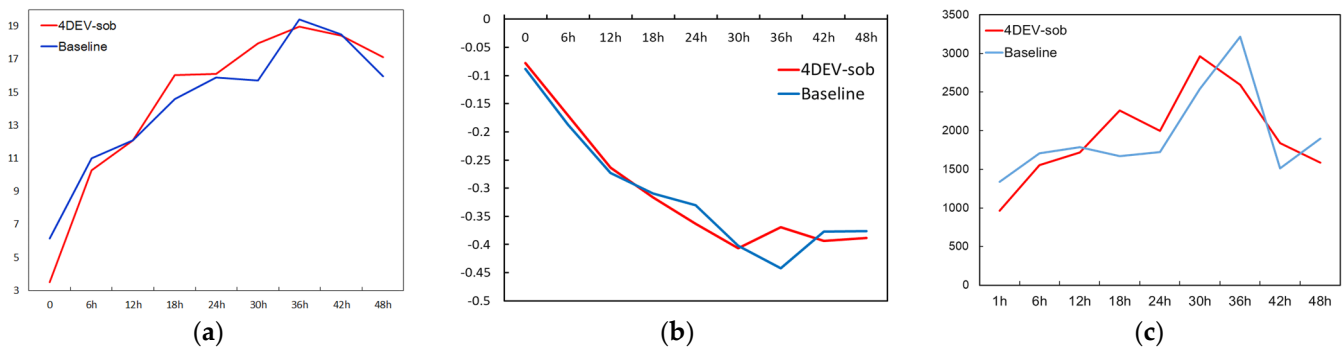
**Figure 7.** The comparison between Baseline (blue line) and 4DEV-sob (red line): (**a**) the strength of upper-level outflow (unit: $10^{-5}$/s) (averaged over 500 km radius); (**b**) the strength of low-level moisture inflow (unit: $10^{-4}$ g/kg.s, averaged over 500 km radius); (**c**) the number of CBs (w > 3 m/s, in 200 km × 200 km × 14 km within 100 km radius). The blue line presents the experiment Baseline and the red presents the experiment 4DEV-sob.

Assimilating HDOB and AMV correctly weakens the upper-level outflow, both for low-level and mid-level inflow and moisture in the USL quadrant in the analysis field (Figures 8a, 9a and 10a). Especially, the outflow is much weaker near the hurricane center than in the Baseline (Figure 9b). Additionally, less water vapor in the USL quadrant is transported into the inner core in the mid-level in experiment 4DEV-sob. However, moisture increases in the inner core above 850 hPa in the USL quadrant. Similarly, assimilating HDOB and AMV also weakens the upper-level outflow and low-level moisture in the DSL analysis (Figures 8b, 9b and 10b). In addition, the temperature of the inner core reduces, resulting in a weaker warm core after assimilation than in the Baseline. Therefore, assimilating HDOB and AMV can improve both the inner-core vortex (such as reducing the low-level moisture and inflow) and the environmental conditions (such as upper-level outflow), especially in the USL and DSL quadrants, providing more realistic low-level inner-core and environmental TC structures.
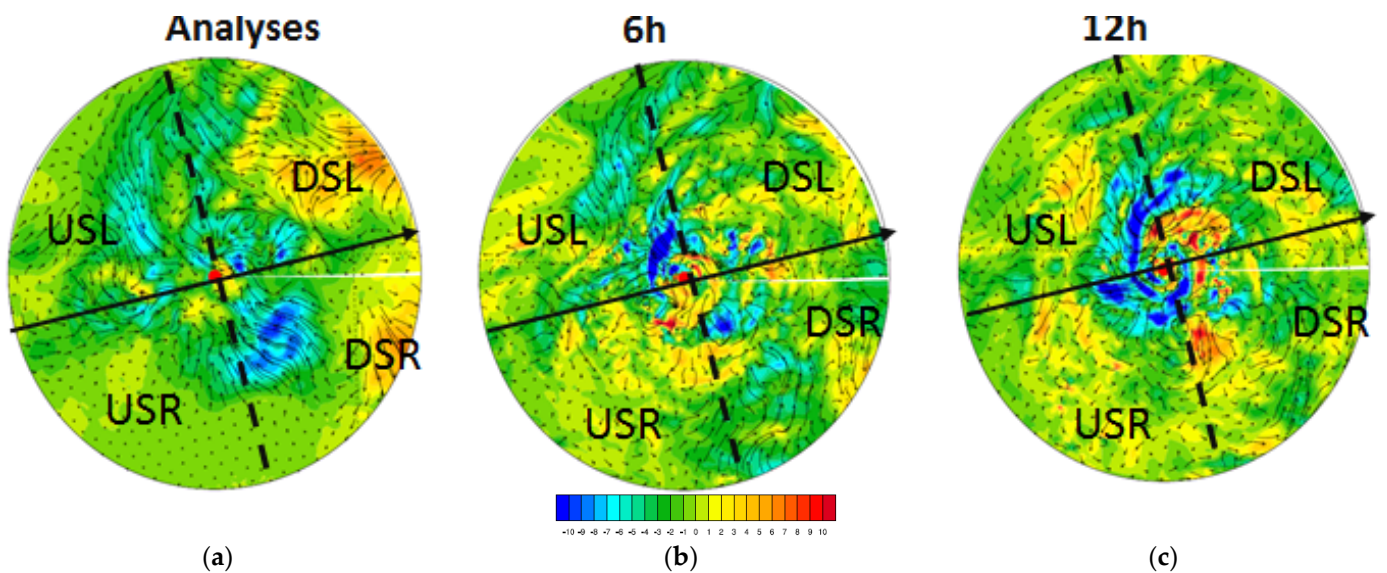


**Figure 8.** Difference of 200 hPa wind field and Vr (radial wind, shaded, unit: m/s) between the experiments 4DEV and Baseline. (**a**) Analyses (0 h); (**b**) 6 h; (**c**) 12 h.
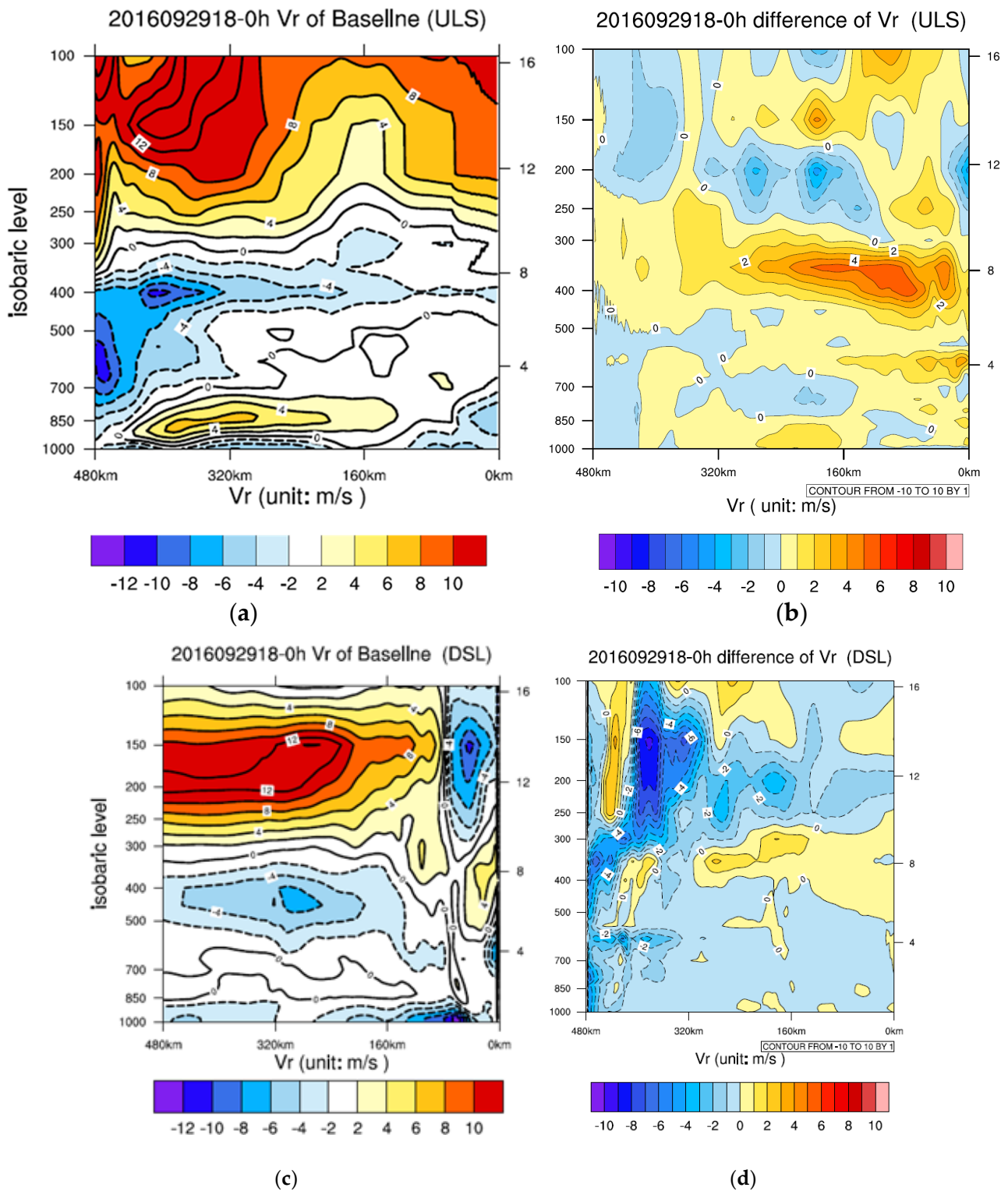
**Figure 9.** The radial wind for the experiment Baseline (**a**,**c**) and the difference of radial wind between experiments 4DEV-sob and Baseline, (**b**,**d**) in USL and DSL.
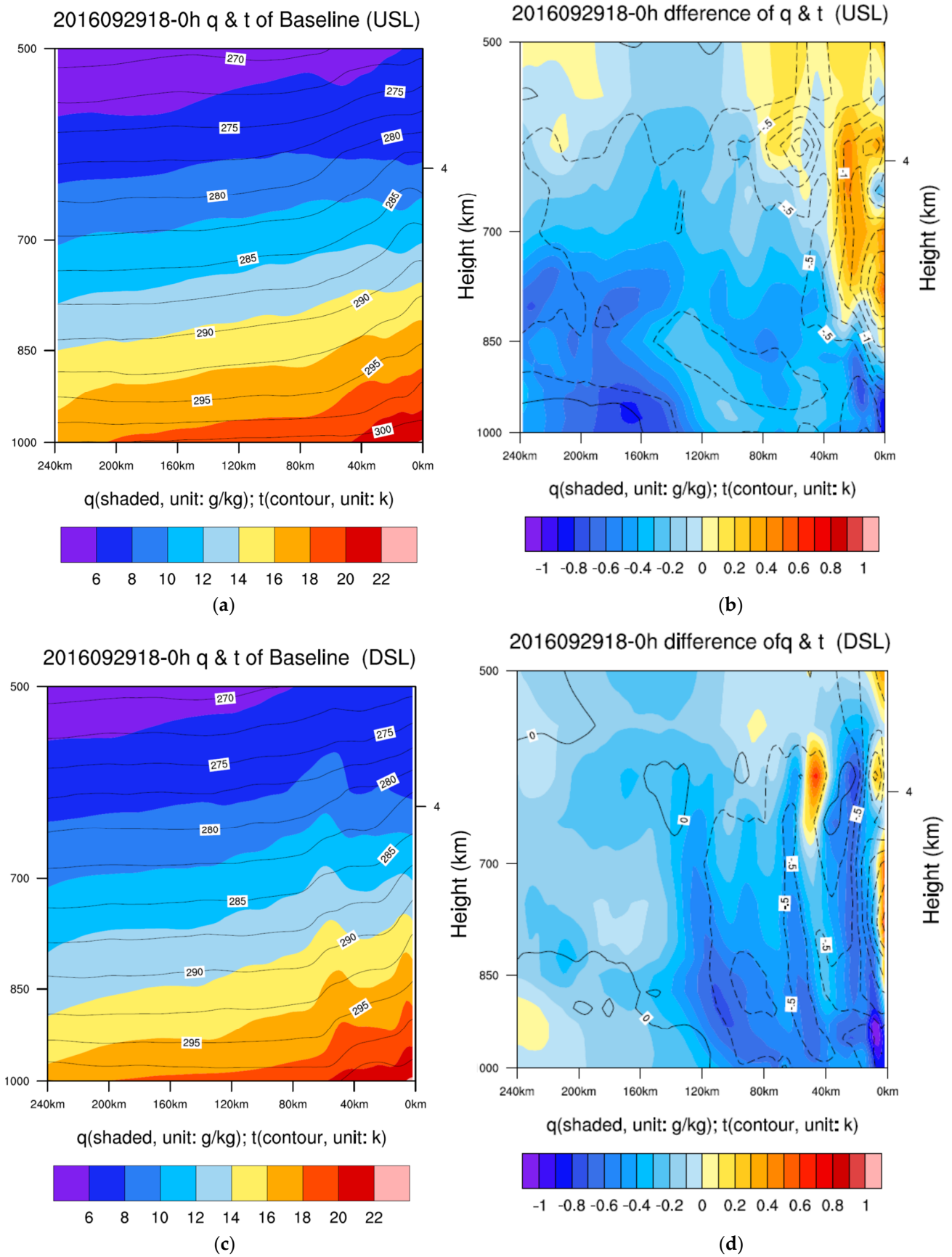
**Figure 10.** The moisture distribution for the experiment Baseline (**a**,**c**) and the difference of moisture between experiments 4DEV and Baseline (**b**,**d**) in USL and DSL.

### 5.2. The Impact of Assimilating HDOB and AMV on the RI forecast

In this section, the impact of assimilating HDOB and AMV observations on the RI prediction is discussed by analyzing the improvement of the shear-relative distribution of environmental conditions and its impact on physical processes of intensification. The RI prediction of 4DEV-sob is close to the observation (Figure 11a), but the intensification rate of Baseline is much higher than both the observation and 4DEV-sob in the first 12 h (over-prediction) (Figure 11). However, the intensification rate of Baseline is lower than both the observation and 4DEV-sob after 12 h (under-prediction). Moreover, the intensification rate of 4DEV-sob is consistent with the observation in the first 24 h (Figure 11b) and the time of peak intensity occurs at the same time as the observation.
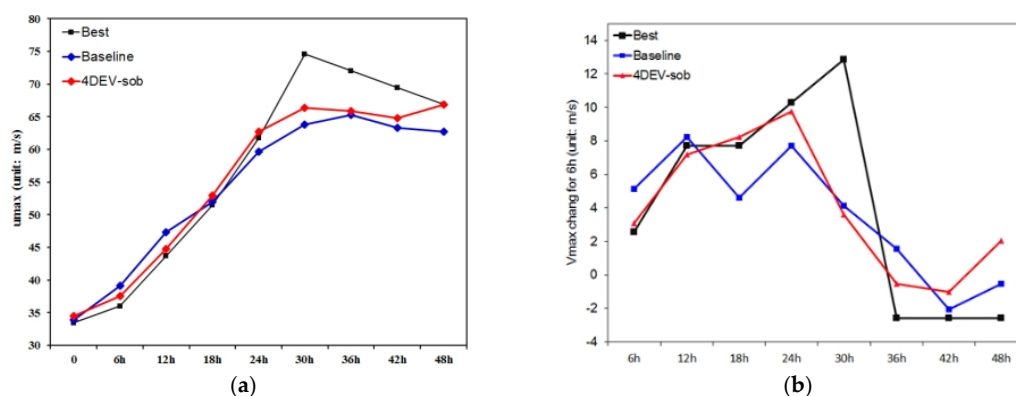


**Figure 11.** Vmax forecasts (**a**) and Vmax change (**b**) for 6 h intervals for 4DEV-sob (red) and Baseline (blue) initialized from 18 UTC 29 September 2016; the black line is for the best track.

From the above discussion, the assimilation of FL and SFMR changes the shear-relative structure of the inner-core vortex and the environment, especially correctly reducing the low-level moisture and weakening the upper-level outflow in the USL and DSL quadrants in the analysis fields for 4DEV-sob. Additionally, the low-level moisture is greater, and upper-level outflow is stronger in Baseline than in 4DEV-sob, causing stronger convergence at the low level and divergence at the upper level in the Baseline than in 4DEV-sob in the first 18 h. Moreover, deep convection in both the DSL and USL quadrants is stronger and the total number of CBs is higher for the Baseline (Figures 7c, Figures 12–14, especially the USL is much stronger than in 4DEV-sob for the first 18 h (Figures 14 and 15).

Further diagnostics show that CBs are stronger in the DSL and USL quadrants in the Baseline than in 4DEV-sob, causing subsidence warming to occur faster before the first 18 h, especially on the left side (including the DSL and USL quadrants) and maximized in the upshear left (Figure 16). Additionally, the positive temperature anomaly in the USL quadrant is higher than in the other three quadrants, subsequently resulting in a larger pressure gradient than in the other three quadrants. Furthermore, the wind distribution of Hurricane Matthew also shows a significant asymmetric structure, with the wind on the left-shear side being much stronger than on the right-shear side (Figure 15). And the location of Vmax moves from the DSL to USL, and the wind in the USL quadrant increases faster than other quadrants for the Baseline, representing the intensity of the hurricane. However, the Vmax in the Baseline is bigger than the best track, causing an over-prediction during the first 18 h. This is consistent with the earlier results of Chen and Gopalakrishnant. Compared with 18 h earlier, the deep convection on the downshear side strengthens and is stronger in the Baseline than in 4DEV-sob after 18 h, expanding cyclonically to the USL quadrant, and then most of the deep convection mainly concentrates on the dowshear side and left-shear side. The asymmetry of the deep convection results in different subsidence warming in the four quadrants. The subsidence warming accelerates in 4DEV-sob, especially on the left-shear side, while it is cut off for a short time, causing under-forecasting in the Baseline. The warm anomaly region on the left side, especially in the USL quadrant, becomes much more significant. Subsequently, the Vmax increases more

rapidly on the left side than in the Baseline and extreme RI occurs. Particularly, the Vmax increases faster in USL quadrant and then it is almost the same or even stronger in the USL than DSL; the intensification rate of 4DEV-sob is more consistent with the best track.
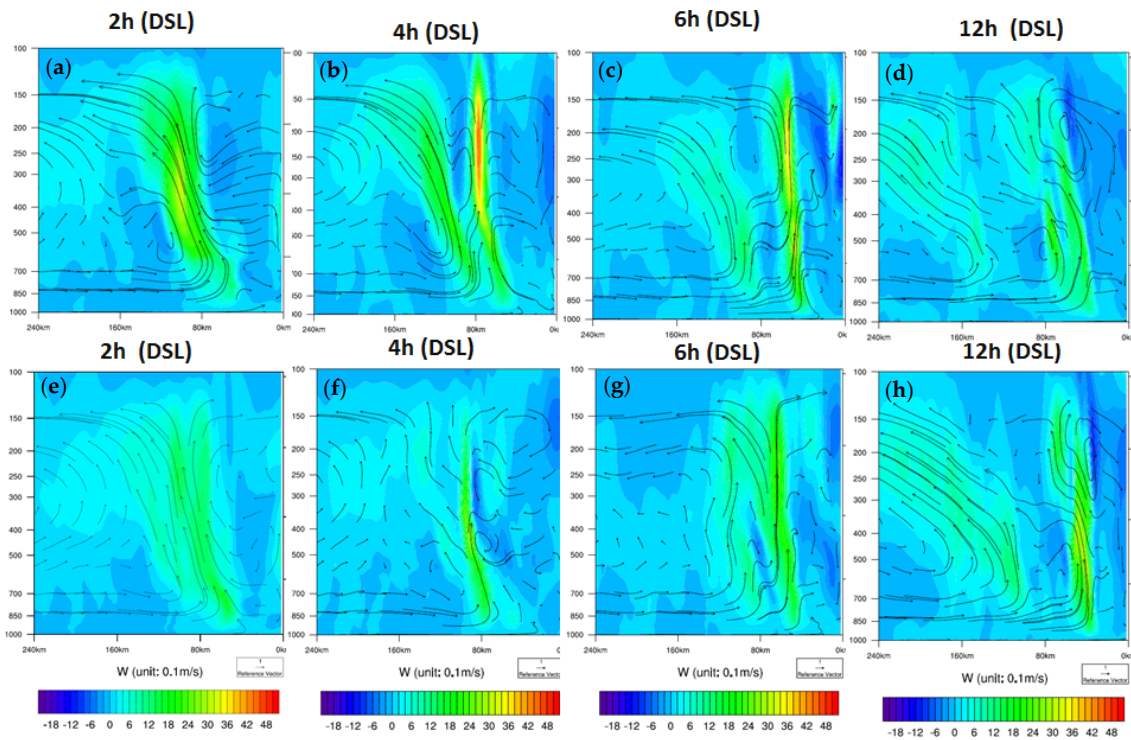


**Figure 12.** The vertical wind of DSL (shaded, unit: 0.1 m/s), the first row is Baseline (**a–d**), the second row is 4DEV-sob (**e–h**).
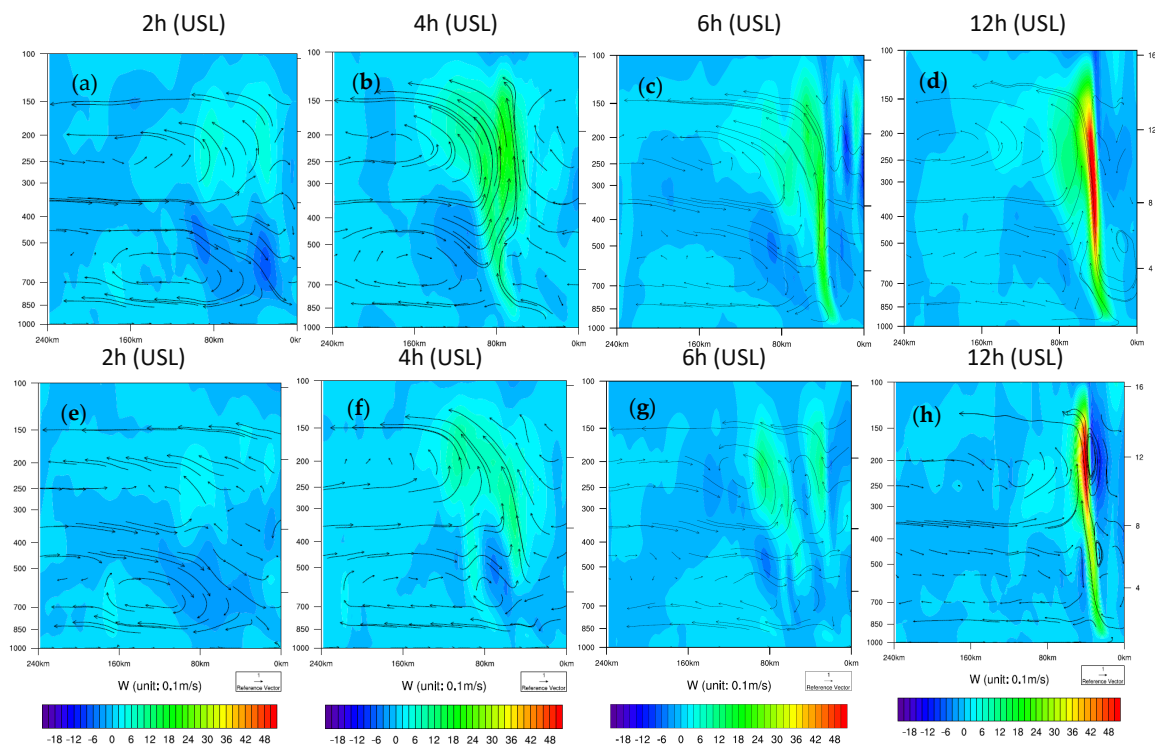


**Figure 13.** The vertical wind of USL (shaded), the first row is Baseline (**a–d**), the second row is. 4DEV-sob (**e–h**).
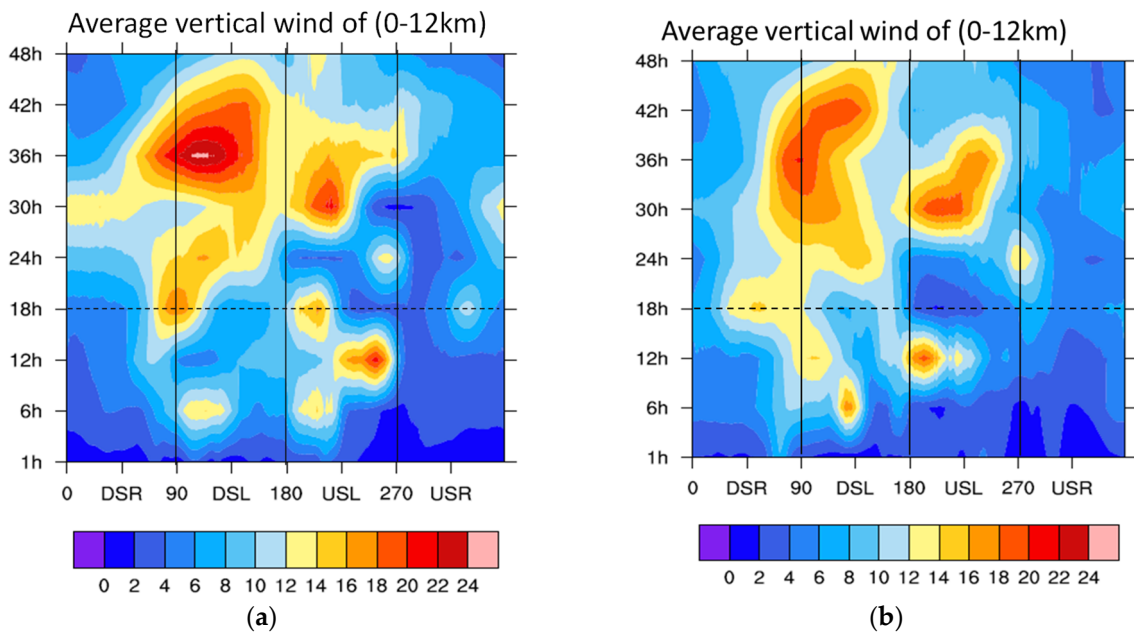
**Figure 14.** The distribution of average vertical wind (averaged over 100 km radius) in the shear-relative quadrants of experiment Baseline (**a**) and 4DEV-sob (**b**).
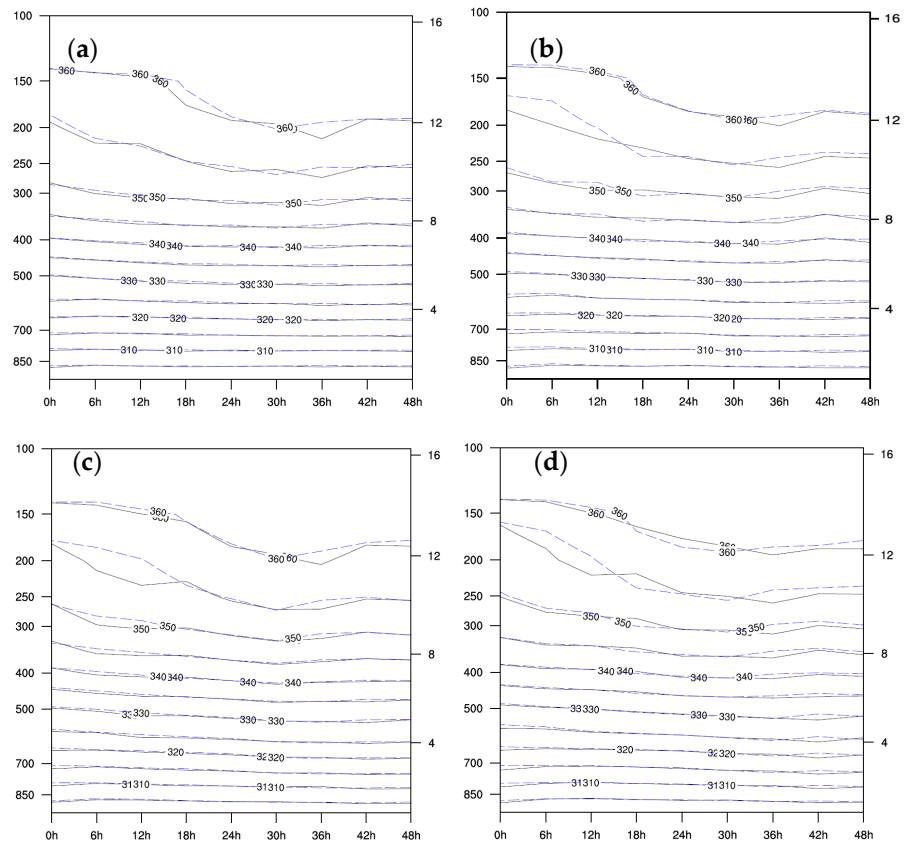


**Figure 15.** Potential temperature (unit: K, averaged over 40 km radius) in the shear-relative quadrants of experiment Baseline (black line) and 4DEV-sob (blue line). (**a**) DSL quadrant, (**b**) DSR quadrant, (**c**) USL quadrant, (**d**) USR quadrant.
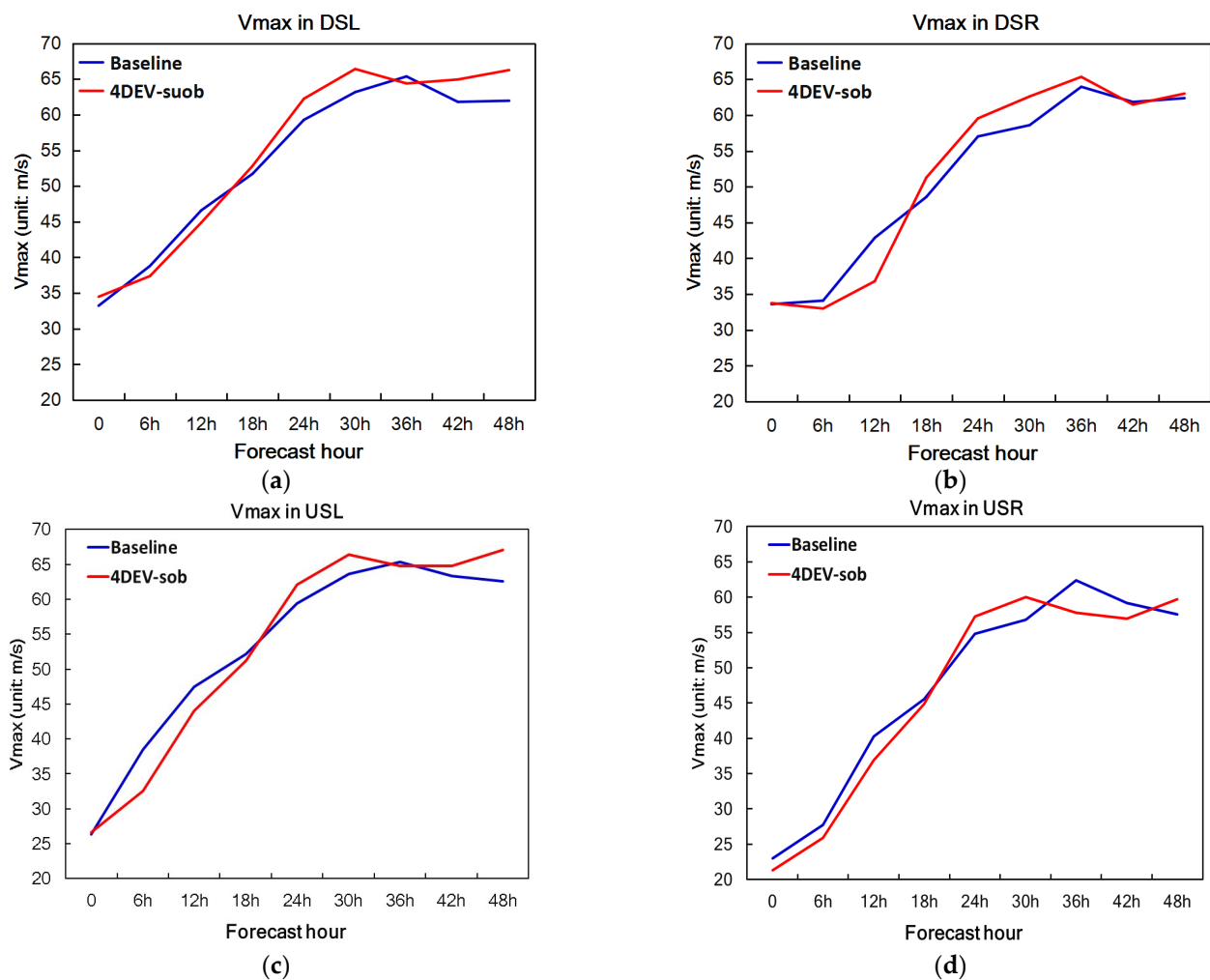
**Figure 16.** The maximum wind (unit: m/s) in the shear-relative quadrants of experiment Baseline (blue line) and 4DEV-sob (red line). (**a**) DSL quadrant, (**b**) DSR quadrant, (**c**) USL quadrant, (**d**) USR quadrant.

In summary, the Baseline experiment over-predicts the RI without assimilating the HDOB and AMV data, while under-forecasting occurs after 18 h. But the assimilation of HDOB and CIMMS AMV correctly weakens the upper-level outflow and changes the structure of the inner-core vortex, such as reducing the low-level moisture and then weakening deep convection, especially in the DSL and USL quadrants. This leads to the intensification rate being consistent with the best track and improves the forecast skill of RI. Therefore, shear-TC intensification is sensitive to the shear-relative distribution of inner and environmental conditions and assimilation can provide a realistic shear-relative inner core or environment and help improve the prediction of RI. Moreover, these results further show that deep convection is highly asymmetric in the process of shear-TC rapid intensification, and the cyclonic movement of that convection from downshear to upshear, especially CBs in the USL quadrant, is key for RI occurrence, and this feature is consistent with early studies [29,38].

## 6. Conclusions and Discussion

Hurricane rapid intensification prediction remains a big challenge in numerical weather prediction. Hurricane Matthew (2016) underwent extreme rapid intensification, intensifying from a Category 1 storm to a Category 5 hurricane within 24 h, despite in a strong shear environmental condition. Most models failed to accurately predict this rapid intensification event. This study aims to investigate the optimal methods for pre-processing

and assimilating HDOB (including FL and SFMR) and CIMMS AMV observations using an advanced cycling hybrid EnVar DA system, and diagnose the impact of assimilating these observations on the prediction of Matthew's RI.

4DEnVar outperforms 3DEnVar without producing a spurious secondary eyewall in the intensity forecast. Additionally, utilizing proper pre-processing techniques (both of thinning and superobbing) for HDOB observations with a 4DEnVar DA method further improves both the analysis and intensity forecast. Notably, the superobbing outperforms thinning, resulting in a RI prediction that is more consistent with the best track without spin-down for the first 24 h, and enhances both the magnitude and timing of the peak intensity. Therefore, with proper pre-processing (thinning or superobbing) of the HDOB observations, the 4DEnVar method enhances the inner-core structure analysis while mitigating the occurrence of the spurious secondary eyewall and spin-down issues.

During the first 18 h, the assimilation of FL and SFMR, along with CIMMS AMV, correctly weakens the upper-level outflow, particularly in the USL quadrant, and changes the shear-relative structure of the inner-core vortex by reducing the low-level moisture and inflow, particularly in the DSL quadrant. Consequently, convection, especially in the DSL and USL quadrants, is weaker compared to the Baseline. However, the stronger convection in these quadrants leads to over-prediction in the Baseline. After 18 h, the deep convection strengthens on the downshear side with assimilation of observations, moving cyclonically to upshear in the left quadrant. This movement results in an increase, maximized in the USL quadrant, and accelerates the maximum wind speed compared to Baseline. Consequently, the intensification rate becomes more consistent with the best track. However, without assimilation, the enhancement of deep convection diminishes, especially in the USL quadrant, leading to under-forecasting in the Baseline. Therefore, while the Baseline experiment without assimilating the HDOB and AMV data over-predicts the RI during the first 18 h, under-forecasting occurs after 18 h. With assimilation, the RI prediction improves and becomes more consistent with the best track.

Hurricane RI prediction remains a significant challenge in numerical weather prediction, particularly in cases of unexpected RI in moderate or strong shear environments, which adds to the difficulty and increases uncertainty. The results of this study suggest that shear-TC intensification is sensitive to the shear-relative distribution of both the inner core and environmental conditions. Proper assimilation can provide a realistic shear-relative inner core or environment, further enhancing the RI forecast skill of the numerical models. Overall, the observations are necessary for improving the prediction of unexpected shear-TC RI. Moreover, these findings further highlight the highly asymmetric nature of deep convection during shear-TC intensification, with deepest convection concentrated on the dowshear and left-shear sides. The cyclonic movement of deep convection from downshear to upshear, especially in the USL quadrant, plays a crucial role in RI occurrence. However, these conclusions are based solely on one storm and one cycle, and more runs and statistics are needed to come up with robust conclusions.

**Author Contributions:** Conceptualization, X.L. and X.W.; methodology, X.L.; software, X.L.; validation, X.L.; formal analysis, X.L.; investigation, X.L. and X.W.; resources, X.W.; data curation, X.L.; writing—original draft preparation, X.L.; writing—review and editing, X.L. and X.W.; visualization, X.L.; supervision, X.W.; project administration, X.W.; funding acquisition, X.W. All authors have read and agreed to the published version of the manuscript.

**Institutional Review Board Statement:** Not applicable.

**Informed Consent Statement:** Not applicable.

**Data Availability Statement:** The data presented in this study are available on request from the corresponding author. The data are not publicly available due to the project.

## References

1.  Kaplan, J.; DeMaria, M.; Knaff, J.A. A revised tropical cyclone rapid intensification index for the Atlantic and eastern North Pacific basins. *Weather Forecast.* **2010**, *25*, 220–241. [CrossRef]
2.  DeMaria, M.; Sampson, C.R.; Knaff, J.A.; Musgrave, K.D. Is tropical cyclone intensity guidance improving? *Bull. Am. Meteorol. Soc.* **2014**, *95*, 387–398. [CrossRef]
3.  Magnusson, L.; Bidlot, J.R.; Bonavita, M.; Brown, A.R.; Browne, P.A.; Chiara, D.G.; Dahoui, M.; Lang, S.T.K.; McNally, T.; Mogensen, K.S.; et al. ECMWF activities for improved hurricane forecasts. *Bull. Am. Meteorol. Soc.* **2019**, *100*, 445–458. [CrossRef]
4.  Wei, N.; McBride, J.L.; Zhang, X.; Duan, Y. Understanding Biases in Tropical Cyclone Intensity Forecast Error. *Weather Forecast.* **2018**, *33*, 129–138.
5.  Poyer, A.; Komaromi, W.; Gopalakrishnan, S.; Wolf, L.; Marks, F.; Alaka, G., Jr.; Anderson, J.; Tallapragada, V.; Brennan, M.; Mehra, A.; et al. *2021–2022 HFIP R&D Activities Summary: Recent Results and Operational Implementation*; HFIP Technical Report; NOAA: Silver Spring, MD, USA, 2023.
6.  Li, Y.; Tang, Y.; Wang, S.; Toumi, R.; Song, X.; Wang, Q. Recent increases in tropical cyclone rapid intensification events in global offshore regions. *Nat. Commun.* **2023**, *14*, 5167. [CrossRef]
7.  Demaria, M.; Kaplan, J. An Updated Statistical Hurricane Intensity Prediction Scheme (SHIPS) for the Atlantic and Eastern North Pacific Basins. *Weather Forecast.* **1999**, *14*, 326–337. [CrossRef]
8.  Paterson, L.A.; Hanstrum, B.N.; Davidson, N.E.; Weber, H.C. Influence of environmental vertical wind shear on the intensity of hurricane-strength tropical cyclones in the Australian region. *Mon. Weather Rev.* **2005**, *133*, 3644–3660. [CrossRef]
9.  Hendricks, E.A.; Peng, M.S.; Fu, B.; Li, T. Quantifying Environmental Control on Tropical Cyclone Intensity Change. *Mon. Weather Rev.* **2010**, *138*, 3243–3271. [CrossRef]
10. Wang, Y.; Rao, Y.; Tan, Z.M.; Schönemann, D. A Statistical Analysis of the Effects of Vertical Wind Shear on Tropical Cyclone Intensity Change over the Western North Pacific. *Mon. Weather Rev.* **2015**, *143*, 3434–3453. [CrossRef]
11. Lyu, X.Y.; Wang, X.; Leslie, L.M. The Dependence of Tropical Cyclone Intensification Rates on the Environmental Factors in the Northwest Pacific Basin. *Adv. Meteorol.* **2019**, *2019*, 9456873. [CrossRef]
12. Gray, W.M. Global View of the Origin of Tropical Disturbances and Storms. *Mon. Weather Rev.* **1968**, *96*, 669–700. [CrossRef]
13. Wang, Y.; Wu, C. Current understanding of tropical cyclone structure and intensity changes-A review. *Meteor. Atmos. Phys.* **2004**, *87*, 257–278. [CrossRef]
14. Cram, T.A.; Persing, J.; Montgomery, M.T.; Braun, S.A. A Lagrangian Trajectory View on Transport and Mixing Processes between the Eye, Eyewall, and Environment Using a High-Resolution Simulation of Hurricane Bonnie (1998). *J. Atmos. Sci.* **2007**, *64*, 1835–1856. [CrossRef]
15. Tang, B.; Emanuel, K. Sensitivity of tropical cyclone intensity to ventilation in an axisymmetric model. *J. Atmos. Sci.* **2012**, *69*, 2394–2413. [CrossRef]
16. Riemer, M.; Montgomery, M.T.; Nicholls, M.E. A New Paradigm for Intensity Modification of Tropical Cyclones: Thermodynamic Impact of Vertical Wind Shear on the Inflow Layer. *Atmos. Chem. Phys.* **2010**, *10*, 3163–3188. [CrossRef]
17. Chen, H.; Gopalakrishnan, S.G. A Study on the Asymmetric Rapid Intensification of Hurricane Earl (2010) Using the HWRF System. *J. Atmos. Sci.* **2015**, *72*, 531–550. [CrossRef]
18. Rios-Berrios, R.; Torn, R.D.; Davis, C.A. An Ensemble Approach to Investigate Tropical Cyclone Intensification in Sheared Environments. Part I: Katia (2011). *J. Atmos. Sci.* **2016**, *73*, 71–93. [CrossRef]
19. Rios-Berrios, R.; Torn, R.D.; Davis, C.A. An Ensemble Approach to Investigate Tropical Cyclone Intensification in Sheared Environments. Part II: Ophelia (2011). *J. Atmos. Sci.* **2016**, *73*, 1555–1575. [CrossRef]
20. Rios-Berrios, R.; Torn, R. Climatological analysis of tropical cyclone intensity changes under moderate vertical wind shear. *Mon. Weather Rev.* **2017**, *145*, 1717–1738. [CrossRef]
21. Emanuel, K.; Desautels, C.; Holloway, C.; Korty, R. Environmental Control of Tropical Cyclone Intensity. *J. Atmos. Sci.* **2004**, *61*, 843–858. [CrossRef]
22. Zhang, F.; Tao, D. Effects of vertical wind shear on the predictability of tropical cyclones. *J. Atmos. Sci.* **2013**, *70*, 975–983. [CrossRef]
23. Tao, D.; Zhang, F. Effects of vertical wind shear on the predictability of tropical cyclones: Practical versus intrinsic limit. *J. Adv. Model. Earth Syst.* **2015**, *7*, 1534–1553. [CrossRef]
24. Bhatia, K.T.; Nolan, D.S. Relating the skill of tropical cyclone intensity forecasts to the synoptic environment. *Weather Forecast.* **2013**, *28*, 961–980. [CrossRef]
25. Gu, J.F.; Tan, Z.M.; Qiu, X. Quadrant-Dependent Evolution of Low-Level Tangential Wind of a Tropical Cyclone in the Shear Flow. *J. Atmos. Sci.* **2016**, *73*, 1159–1177. [CrossRef]
26. Gu, J.F.; Tan, Z.M.; Qiu, X. The evolution of vortex tilt and vertical motion of tropical cyclones in directional shear flows. *J. Atmos. Sci.* **2018**, *75*, 3565–3578. [CrossRef]

27.    Hazelton, A.; Alaka, G.J., Jr.; Cowan, L.; Fischer, M.; Gopalakrishnan, S. Understanding the Processes Causing the Early Intensification of Hurricane Dorian through an Ensemble of the Hurricane Analysis and Forecast System (HAFS). *Atmosphere* **2021**, *12*, 93. [CrossRef]

28.    Zawislak, J.; Jiang, H.; Alvey, G.R.; Zipser, E.J.; Rogers, R.F.; Zhang, J.A.; Stevenson, S.N. Observations of the structure and evolution of Hurricane Edouard (2014) during intensity change. Part I: Relationship between the thermodynamic structure and precipitation. *Mon. Weather Rev.* **2016**, *144*, 3333–3354. [CrossRef]

29.    Leighton, H.; Gopalakrishnan, S.; Zhang, J.A.; Rogers, R.F.; Zhang, Z.; Tallapragada, V. Azimuthal Distribution of Deep Convection, Environmental Factors, and Tropical Cyclone Rapid Intensification: A Perspective from HWRF Ensemble Forecasts of Hurricane Edouard (2014). *J. Atmos. Sci.* **2018**, *75*, 275–295. [CrossRef]

30.    Shu, S.; Wu, L. Analysis of the influence of Saharan air layer on tropical cyclone intensity using AIRS/Aqua data. *Geophys. Res. Lett.* **2009**, *36*, L09809. [CrossRef]

31.    Wu, T.C.; Liu, H.; Majumdar, S.J.; Velden, C.S.; Anderson, J.L. Influence of assimilating satellite-derived atmospheric motion vector observations on numerical analyses and forecasts of tropical cyclone track and intensity. *Mon. Weather Rev.* **2014**, *142*, 49–71. [CrossRef]

32.    Wu, T.C.; Velden, C.S.; Majumdar, S.J.; Liu, H.; Anderson, J.L. Understanding the influence of assimilating subsets of enhanced atmospheric motion vectors on numerical analyses and forecasts of tropical cyclone track and intensity with an ensemble Kalman filter. *Mon. Weather Rev.* **2015**, *143*, 2506–2531. [CrossRef]

33.    Nguyen, L.T.; Molinari, J. Rapid intensification of a sheared, fast-moving hurricane over the Gulf Stream. *Mon. Weather Rev.* **2012**, *140*, 3361–3378. [CrossRef]

34.    Zhang, J.A.; Rogers, R.F.; Reasor, P.D.; Uhlhorn, E.W.; Marks, F.D. Asymmetric Hurricane Boundary Layer Structure from Dropsonde Composites in Relation to the Environmental Vertical Wind Shear. *Mon. Weather Rev.* **2013**, *141*, 3968–3984. [CrossRef]

35.    Stevenson, S.N.; Corbosiero, K.L.; Demaria, M.; Vigh, J.L. A 10-Year Survey of Tropical Cyclone Inner-Core Lightning Bursts and Their Relationship to Intensity Change. *Weather Forecast.* **2018**, *33*, 23–36. [CrossRef]

36.    Molinari, J.; Vollaro, D. Rapid Intensification of a Sheared Tropical Storm. *Mon. Weather Rev.* **2010**, *138*, 3869–3885. [CrossRef]

37.    Chen, B.F.; Davis, C.A.; Kuo, Y.H. Effects of Low-Level Flow Orientation and Vertical Shear on the Structure and Intensity of Tropical Cyclones. *Mon. Weather Rev.* **2018**, *146*, 2447–2467. [CrossRef]

38.    Wadler, J.B.; Rogers, R.F.; Reasor, P.D. The relationship between spatial variations in the structure of convective bursts and tropical cyclone intensification as determined by airborne Doppler radar. *Mon. Weather Rev.* **2018**, *146*, 761–780. [CrossRef]

39.    Fischer, M.S.; Tang, B.H.; Corbosiero, K.L.; Rozoff, C.M. Normalized convective characteristics of tropical cyclone rapid intensification events in the North Atlantic and eastern North Pacific. *Mon. Weather Rev.* **2018**, *146*, 1133–1155. [CrossRef]

40.    Weng, Y.; Zhang, F. Assimilating airborne Doppler radar observations with an ensemble Kalman filter for convection-permitting hurricane initialization and prediction: Katrina (2005). *Mon. Weather Rev.* **2012**, *140*, 841–859. [CrossRef]

41.    Rogers, R.; Uhlhorn, E. Observations of the structure and evolution of surface and flight-level wind asymmetries in Hurricane Rita (2005). *Geophys. Res. Lett.* **2008**, *35*, L22811. [CrossRef]

42.    Uhlhorn, E.W.; Black, P.G.; Franklin, J.L.; Goodberlet, M.; Carswell, J.; Goldstein, A.S. Hurricane surface wind measurements from an operational stepped frequency microwave radiometer. *Mon. Weather Rev.* **2007**, *135*, 3070–3085. [CrossRef]

43.    Lu, X.; Wang, X. Improving hurricane analyses and predictions with TCI, IFEX field campaign observations, and CIMSS AMVs using the advanced hybrid data assimilation system for HWRF. Part I: What is missing to capture the rapid intensification of Hurricane Patricia (2015) when HWRF is already initialized with a more realistic analysis? *Mon. Weather Rev.* **2019**, *147*, 1351–1373.

44.    Lu, X.; Wang, X. Improving hurricane analyses and predictions with TCI, IFEX field campaign observations, and CIMSS AMVs using the advanced hybrid data assimilation system for HWRF. Part II: Observation impacts on the analyses and predictions of Patricia (2015). *Mon. Weather Rev.* **2020**, *148*, 1407–1430. [CrossRef]

45.    Willoughby, H.E.; Chelmow, M.B. Objective determination of hurricane tracks from aircraft observations. *Mon. Weather Rev.* **1982**, *110*, 1298–1305. [CrossRef]

46.    Willoughby, H.E.; Rahn, M.E. Parametric representation of the primary Hurricane Vortex. Part I: Observations and evaluation of the Holland (1980) model. *Mon. Weather Rev.* **2004**, *132*, 3033–3048. [CrossRef]

47.    Aksoy, A.; Aberson, S.D.; Vukicevic, T.; Sellwood, K.J.; Lorsolo, S.; Zhang, X. Assimilation of high-resolution tropical cyclone observations with an ensemble Kalman filter using NOAA/AOML/HRD's HEDAS: Evaluation of the 2008–11 vortex-scale Analyses. *Mon. Weather Rev.* **2013**, *141*, 1842–1865. [CrossRef]

48.    Velden, C.; Lewis, W.E.; Bresky, W.; Stettner, D.; Daniels, J.; Wanzong, S. Assimilation of high-resolution satellite-derived atmospheric motion vectors: Impact on HWRF forecasts of tropical cyclone track and intensity. *Mon. Weather Rev.* **2017**, *145*, 1107–1125. [CrossRef]

49.    Velden, C.S.; Olander, T.L.; Wanzong, S. The Impact of Multispectral GOES-8 Wind Information on Atlantic Tropical Cyclone Track Forecasts in 1995. Part I: Dataset Methodology, Description, and Case Analysis. *Mon. Weather Rev.* **1998**, *126*, 1202–1218. [CrossRef]

50.    Elsberry, R.L.; Buholzer, N.; Velden, C.S.; Jordan, M.S. Satellite-Based Observations of Nonlinear Relationships between Vertical Wind Shear and Intensity Changes during the Life Cycle of Hurricane Joaquin (2015). *Weather Forecast.* **2020**, *35*, 939–958. [CrossRef]

51. Cherubini, T.; Businger, S.; Velden, C.; Ogasawara, R. The Impact of Satellite-Derived Atmospheric Motion Vectors on Mesoscale Forecasts over Hawaii. *Mon. Weather Rev.* **2006**, *134*, 2009–2020. [CrossRef]

52. Langland, R.H.; Velden, C.; Pauley, P.M.; Berger, H. Impact of satellite-derived rapid-scan wind observations on numerical model forecasts of Hurricane Katrina. *Mon. Weather Rev.* **2009**, *137*, 1615–1622. [CrossRef]

53. Berger, H.; Langland, R.; Velden, C.S.; Reynolds, C.A.; Pauley, P.M. Impact of Enhanced Satellite-Derived Atmospheric Motion Vector Observations on Numerical Tropical Cyclone Track Forecasts in the Western North Pacific during TPARC/TCS-08. *J. Appl. Meteor. Climatol.* **2011**, *50*, 2309–2318. [CrossRef]

54. Wang, X.; Barker, D.; Snyder, C.; Hamill, T.M. A hybrid ETKF–3DVAR data assimilation scheme for the WRF model. Part I: Observing system simulation experiment. *Mon. Wea. Rev.* **2008**, *136*, 5116–5131. [CrossRef]

55. Wang, X.; Barker, D.; Snyder, C.; Hamill, T.M. A hybrid ETKF–3DVAR data assimilation scheme for the WRF model. Part II: Real observation experiments. *Mon. Wea. Rev.* **2008**, *136*, 5132–5147. [CrossRef]

56. Wang, X. Incorporating ensemble covariance in the Gridpoint Statistical Interpolation variational minimization: A mathematical framework. *Mon. Wea. Rev.* **2010**, *138*, 2990–2995. [CrossRef]

57. Wang, X.; Parrish, D.; Kleist, D.; Whitaker J., S. GSI 3DVar-based ensemble–variational hybrid data assimilation for NCEP Global Forecast System: Single-resolution experiments. *Mon. Wea. Rev.* **2013**, *141*, 4098–4117. [CrossRef]

58. Wang, X.; Lei, T. GSI-based four dimensional ensemble-variational (4DEnsVar) data assimilation: Formulation and single resolution experiments with real data for NCEP Global Forecast System. *Mon. Wea. Rev.* **2014**, *142*, 3303–3325. [CrossRef]

59. Lu, X.; Wang, X.; Tong, M.; Tallapragada, V. GSI-based, continuously cycled, dual-resolution hybrid ensemble-variational data assimilation system for HWRF: System description and experiments with Edouard (2014). *Mon. Wea. Rev.* **2017**, *145*, 4877–4898. [CrossRef]

60. Lorenc, A.C.; Rawlins, F. Why does 4D-Var beat 3D-Var? *Q. J. R. Meteorol. Soc.* **2010**, *131*, 3247–3257. [CrossRef]

61. Zhang, M.; Zhang, F. E4DVar: Coupling an Ensemble Kalman Filter with Four-Dimensional Variational Data Assimilation in a Limited-Area Weather Prediction Model. *Mon. Weather Rev.* **2011**, *140*, 587–600. [CrossRef]

62. Stewart, S.R. National Hurricane Center Tropical Cyclone Report: Hurricane Matthew (AL 142016). 2017. Available online: https://www.nhc.noaa.gov/data/tcr/AL142016_Matthew.pdf (accessed on 24 December 2023).

63. Liu, Z.; Rabier, F. The interaction between model resolution, observation resolution and observation density in data assimilation: A one-dimensional study. *Q. J. R. Meteorol. Soc.* **2002**, *128*, 1367–1386. [CrossRef]